
High-Resolution Near-Field Raman Microscopy of Single-Walled Carbon Nanotubes

Introduction

Recent rapid advances in nanotechnology and nanoscience are largely due to our newly acquired ability to measure and manipulate individual structures on the nanoscale. Among the new methods are scanning probe techniques, optical tweezers, and high-resolution electron microscopes. A recently demonstrated near-field optical technique allows spectroscopic measurements with 20-nm spatial resolution.¹ This method makes use of the strongly enhanced electric field close to a sharp metal tip under laser illumination and relies on the detection of two-photon excited fluorescence. Fluorescence imaging, however, requires a high fluorescence quantum yield of the system studied or artificial labeling with fluorophores. Furthermore, fluorescence quenching by the metal tip competes with the local field enhancement effect and therefore limits the general applicability. On the other hand, Raman scattering probes the unique vibrational spectrum of the sample and directly reflects its chemical composition and molecular structure. A main drawback of Raman scattering is the extremely low scattering cross section, which is typically 14 orders of magnitude smaller than the cross section of fluorescence. Surface-enhanced Raman scattering (SERS), induced by nanometer-sized metal structures, has been shown to provide enormous enhancement factors of up to 10^{15} , allowing for Raman spectroscopy even on the single-molecule level.^{2,3} Controlling SERS with a sharp metal tip that is raster scanned over a sample surface has been proposed in Refs. 1 and 4, and near-field Raman enhancement has been experimentally demonstrated in Refs. 5–9. Here, we show the chemical specificity of this near-field technique and demonstrate an unprecedented spatial resolution.

Single-walled carbon nanotubes (SWNT's) have been the focus of intense interest due to a large variety of potential nanotechnological applications. The unique properties of SWNT's arise from their particular one-dimensional structure, which is directly linked to the characteristic Raman bands. Raman scattering on SWNT's has been studied intensively in the literature (see, e.g., Refs. 10–13), and Raman enhancements of up to 10^{12} have been reported for tubes in contact with fractal silver colloidal clusters.¹⁴ In this article, near-field

Raman imaging of SWNT's is demonstrated using a sharp silver tip as a probe. We show, for the first time, that single isolated SWNT's can be detected optically with a spatial resolution of better than 30 nm. This high-resolution capability is applied to resolve local variations in the Raman spectrum along a single SWNT that would be hidden in far-field measurements. The near-field origin of the Raman enhancement is proven by tip-to-sample-distance measurements.

Experimental

Our experimental setup is based on an inverted optical microscope with an x,y scan stage for raster scanning a transparent sample with SWNT's. A laser beam ($\lambda = 633$ nm, 30 to 100 μW) is reflected by a dichroic beam splitter and focused by a high numerical aperture objective (1.4 N.A.) on the sample surface. A sharp silver tip is positioned near the focus of the beam and maintained above the sample surface at a distance ≈ 1 nm by means of a sensitive shear-force feedback mechanism.¹⁵ Raman-scattered light is collected with the same objective, transmitted by the beam splitter, and filtered by a long pass filter. The signal is detected either by a combination of a spectrograph and a thermoelectrically cooled charge-coupled device (CCD) or by a narrow bandpass filter (FWHM = 10 nm) centered at 760 nm (or 700 nm), followed by a single-photon counting avalanche photodiode. A near-field Raman image is established by raster scanning the sample and continuously recording the scattered Raman signal. Sharp silver tips with a radius of 10 to 15 nm are produced by electrochemical etching followed by focused-ion-beam (FIB) milling with a dual-beam FIB system (FEI Strata-235) and applying a similar procedure as used for STM/AFM tip sharpening.¹⁶

To establish a strong field enhancement at the tip, the electric field of the exciting laser beam needs to be polarized along the tip axis.¹⁷ To achieve this condition in our on-axis illumination scheme, we displace the tip from the center of the beam in the direction of polarization into one of the two longitudinal field lobes characteristic of strongly focused Gaussian beams.¹⁸ The strength of this longitudinal field increases with increasing N.A. of the focusing lens and, in our

configuration, is only five times weaker than the transverse field strength at the center of the focus.

Results and Discussion

Two different types of SWNT samples were studied. The first sample consists of nearly monodisperse SWNT's grown by chemical vapor deposition (CVD) on SiO₂ substrates. The substrates were first cleaned by solvent washing, then heated to 700°C in a tube furnace for 30 min while being exposed to air. Next, 50 μL of Ferritin solution [Sigma-Aldrich; diluted in deionized (DI) water, 1:10 ratio (Ferritin: H₂O)] was applied to the clean substrate, which was left for 30 s, then rinsed with DI water and placed in the tube furnace using growth parameters similar to commonly known SWNT growth methods.¹⁹ The material for the second sample was purchased from Bucky USA and consists of purified SWNT's with a diameter distribution from 1.0 to 1.8 nm, produced by arc discharge using Ni/Y catalyst particles. The material was dispersed in dichloroethane, sonicated for 1 h, and spin-cast onto a microscope cover glass. AFM measurements were performed to determine sample coverage and to distinguish spatially isolated tubes from nanotube bundles.

The far-field Raman spectra of the SWNT samples (not shown) are dominated by the sharp tangential stretching mode at 1596 cm⁻¹ (*G* band) and a broader band around 2615 cm⁻¹ (*G'* band), which arises from an overtone of the disorder-induced mode around 1310 cm⁻¹.²⁰ Figure 93.55 shows confocal far-field Raman images of SWNT bundles produced by

arc discharge that were recorded by integrating the signal intensity of the *G'* band [760-nm bandpass filter (see above)] for vertical (a) and horizontal (b) polarization of the incident laser beam. Similar Raman images are obtained by detecting the intensity of the *G* band using the 700-nm bandpass filter. The Raman images clearly demonstrate that tubes oriented completely perpendicular to the respective light polarization do not produce any signal (see arrows in Fig. 93.55). This polarization contrast is a consequence of the polarization properties of the *G* and *G'* Raman bands reported for *G* in the literature.^{11,12,21} AFM measurements of the same area reveal that the diameter of the nanotube bundles varies between 5 and 15 nm, which corresponds to 10 to 100 individual nanotubes per bundle.

Confocal Raman imaging of SWNT's grown by CVD was not possible within feasible acquisition times because the sample consists mostly of separated individual SWNT's for which the Raman scattering strength is much weaker. However, as shown in Fig. 93.56(a) for CVD-grown SWNT's, the contrast and resolution of Raman images can be greatly increased by positioning a sharp silver tip near the laser focus. The simultaneously recorded topographic image is presented in Fig. 93.56(b). The lower portions [Figs. 93.56(c) and 93.56(d)] show cross sections taken along the dashed white lines. Besides SWNT's, the topographic image shows a large number of small circular features with a height ≈ 2 nm, which are due to condensating water and can be removed by sample heating to 70°C. Comparison of the widths (FWHM) of SWNT's in the topographic and Raman images indicates that the resolution of the Raman image is better than the resolution of the topographic image (25 nm versus 30 nm). This high spatial resolution is unprecedented and clearly indicates the near-field origin of the Raman signal. The width of the optical features and the topographical features results from the convolution of the tip shape with the object studied and is therefore limited by the finite size of the tip apex. Both images are closely correlated and the SWNT's are clearly identified. The small topographic features formed by condensation do not show up, however, in the Raman image, which proves the chemical specificity of the method. The diameter of SWNT's grown by CVD can be controlled by growth parameters. The sample used in Fig. 93.56 consists mostly of SWNT's with a diameter ≈ 1.4 nm, which is verified by the topographic data in Figs. 93.56(b) and 93.56(d) and also by independent AFM measurements in the absence of water condensation. Thus, we observe near-field Raman scattering from spatially separated single SWNT's. It is important to notice that vertically *and* horizontally oriented SWNT's are observed in the Raman

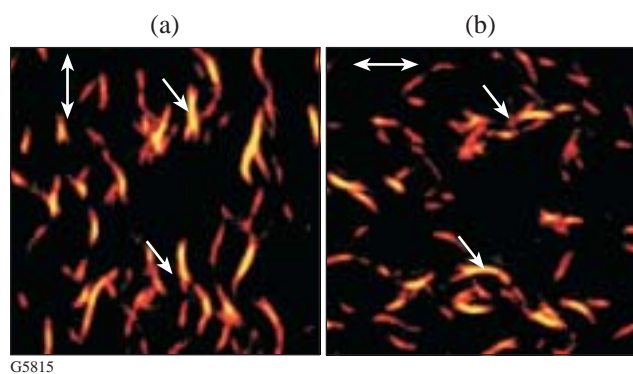
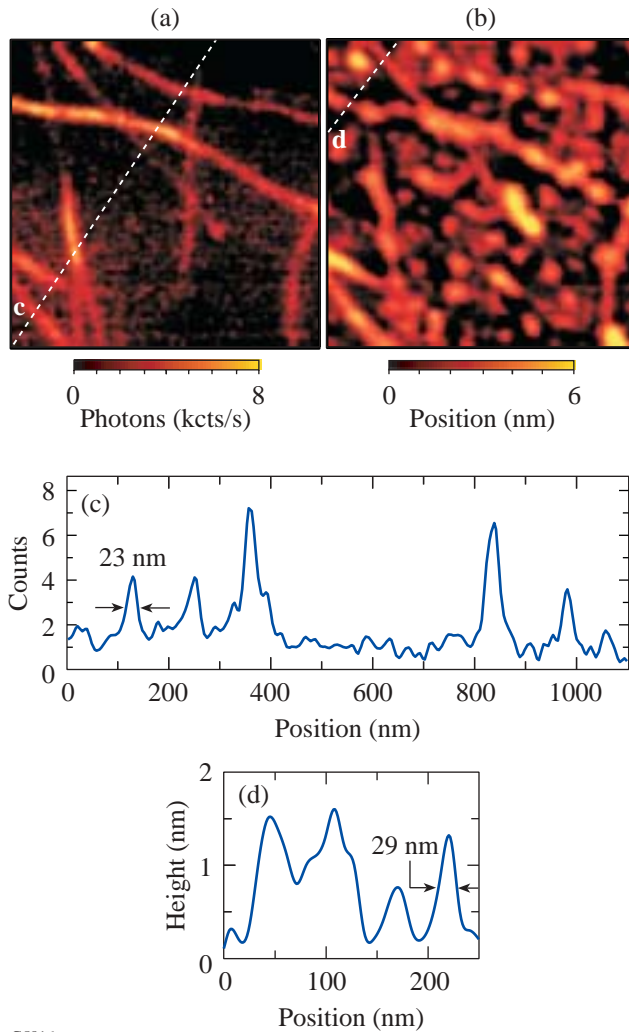


Figure 93.55 Confocal Raman images of SWNT bundles produced by arc discharge on glass acquired by detecting the intensity of the *G'* band ($\nu = 2615 \text{ cm}^{-1}$) while raster-scanning the sample (without metal tip, scan area $15 \times 15 \mu\text{m}$) for vertical (a) and horizontal polarization (b) of the laser excitation at 633 nm. The arrows indicate tubes that are oriented completely perpendicular to one polarization direction, demonstrating the polarization contrast.

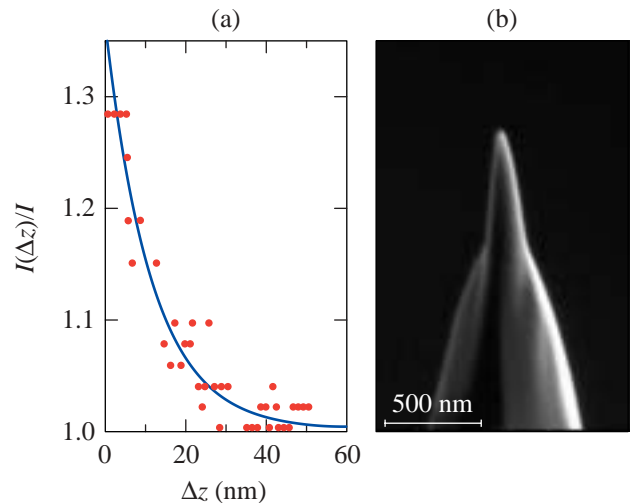
image with similar signal intensity, even though the incident laser light is oriented vertically. This observation is in strong contrast to the polarization contrast observed in the far-field measurements shown in Fig. 93.55. Accordingly, the polarization of the enhanced field has to be radially symmetric with respect to the tip axis. This finding is in agreement with theoretical calculations¹⁷ and confirms the unique properties of the near field.



G5816

Figure 93.56 Simultaneous near-field Raman image (a) and topographic image (b) of SWNT's grown by CVD on glass (scan area $1 \times 1 \mu\text{m}$). The Raman image is acquired by detecting the intensity of the G' band upon laser excitation at 633 nm. No Raman scattering signal is detected from humidity-related circular features present in the topographic image (see text). (c) Cross section taken along the indicated dashed line in the Raman image. (d) Cross section taken along the indicated dashed line in the topographic image. The height of individual tubes is ≈ 1.4 nm. Vertical units are photon counts per second for (c) and nanometer for (d).

The optical resolution apparent in Fig. 93.56 shows that the enhanced field is laterally confined to the size of the metal tip. To demonstrate the confinement of the enhanced fields in the longitudinal direction, the tip is positioned above a SWNT and the Raman scattering strength is recorded as a function of tip-to-sample distance Δz . The result, shown in Fig. 93.57, has been fitted with an exponential curve and normalized with the Raman scattering strength in the absence of the tip, i.e., with the far-field Raman signal. For distances $\Delta z < 30$ nm, the increase of the signal clearly indicates a distance-dependent near-field contribution with a decay length of 11 nm. This longitudinal confinement is in agreement with the lateral confinement observed in the near-field Raman images and consistent with the tip radius of 10 to 15 nm as determined by a scanning electron microscopy [cf. Fig. 93.57(b)]. All of the tips used in our experiments were fabricated by the same procedure and rendered similar SEM images; however, only about 30% to 40% of the tips produced a measurable signal enhancement. The reason for this behavior is the subject of ongoing studies. The highest Raman enhancement factors observed so far were estimated to be around 10^3 . These numbers follow from the detected ratio of near-field to far-field signals and from a comparison of the different volumes probed by the near field and the far field.



G5817

Figure 93.57 (a) Dependence of the Raman-scattering strength of the G' band (I) on the longitudinal separation (Δz) between a single SWNT and the tip. The solid line is an exponential fit with a decay length of 11 nm. The signal is normalized with the far-field signal. (b) Scanning electron micrograph of a sharp silver tip fabricated by focused-ion-beam milling.

To demonstrate the high-resolution spectroscopic capabilities of the near-field technique presented here, we investigate the Raman spectrum along a SWNT with a diameter of 1.7 nm grown by arc discharge. Figure 93.58(a) shows the topography near the end of a SWNT produced by this technique. Three bumps with a height ≈ 5 nm can be recognized on top of the SWNT. Because of their size, these bumps are presumably Ni/Y-catalyst particles, indicating the initial point of growth.²² The labels 1 to 4 in Fig. 93.58(a) mark the positions at which Raman spectra were taken in the presence of the metal tip. At the very beginning of the SWNT (positions 1 and 2) the G band at 1596 cm^{-1} (FWHM = 17 cm^{-1}) dominates the spectra and is significantly stronger than the G' band at 2619 cm^{-1} (FWHM = 35 cm^{-1}) with an amplitude ratio $G/G' \approx 1.3$ [see Fig. 93.58(b)]. Moving along the SWNT to position 3 and farther to position 4 (separated by 35 nm and 85 nm, respectively), however, the amplitude of the G band decreases with respect to the G' band and the ratio G/G' reduces to ~ 0.7 . Simultaneously, the shape of the G' band changes and its center frequency is shifted to 2610 cm^{-1} , whereas the G band re-

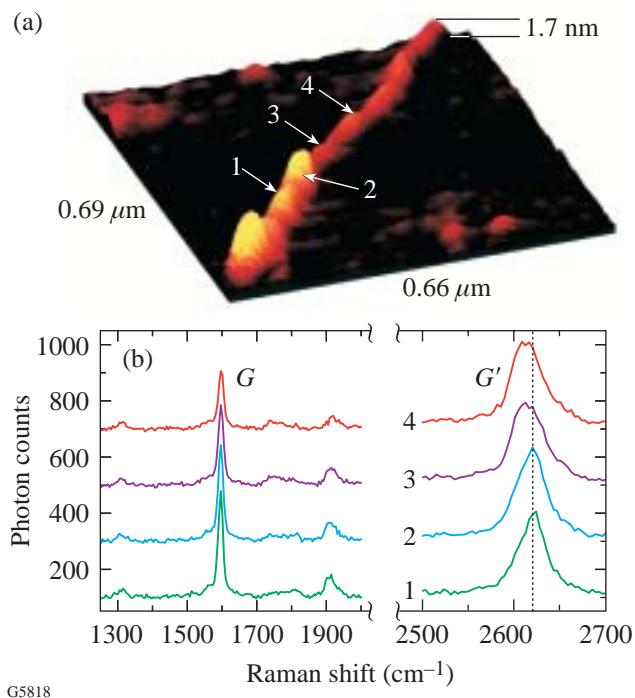


Figure 93.58

(a) Three-dimensional topographic image of a SWNT on glass grown by arc discharge. The three bumps are presumably enclosed Ni/Y catalyst particles and indicate the initial point of growth. (b) Near-field Raman spectra detected at the marked positions 1 to 4 in (a). The distance between positions 2 and 3 is 35 nm. The spectra are offset for clarity.

mains at 1596 cm^{-1} . For 1 and 2, the G' band has a Lorentzian shape, while for 3 and 4, two Lorentzian peaks are needed to model its shape. Raman spectra recorded beyond point 4 in Fig. 93.58(a) remain unchanged.

Variations in the Raman spectrum reflect changes in the molecular structure that can have several origins such as external stress, due to the catalyst particles, or local defects in the tube structure. The observed spectral variations between 2 and 3 can also be explained by a change of the tube structure, described by $(n,m) \rightarrow (n',m')$, which modifies the electronic-state energies of the tube and therefore the resonance enhancement of the Raman bands at a fixed excitation energy. A decrease of the resonance enhancement between positions 2 and 3 would lead to a lower G -band amplitude and could cause a splitting of the G' band into a double peak.²⁰

Recent experiments have shown that huge surface enhancement of Raman signals can be accompanied by fluctuating white-light emission.^{3,23} According to Ref. 23, huge SERS enhancement and strong white-light emission require chemisorption of the Raman scatterer to the metal surface. Since we maintain a well-defined separation (≈ 1 nm) between tip and sample in our experiments, we do not expect a significant white-light contribution. Moreover, white-light emission is observed for Raman enhancement factors more than ten orders of magnitude stronger than the enhancements determined in our experiments. Indeed, our near-field Raman spectra show no indication for a significant broadband background [see Fig. 93.58(b)]. To exclude any contributions to the image contrast arising from background signals, we recorded for each image pixel the full spectrum and integrated the intensity of the G' band and the G band while subtracting the background. The resulting images were virtually identical to those shown in Fig. 93.56(a). We also note that by comparing the near-field and far-field Raman spectra of SWNT's, we find, within the noise limit, no indication for the gradient-field Raman effect discussed in Ref. 24.

Conclusion

We have demonstrated a method for nanoscale Raman spectroscopy with sub-30-nm spatial resolution. This method extends our abilities to characterize weakly fluorescent structures on the nanoscale. Near-field Raman spectroscopy combined with simultaneous AFM measurements appears to be extremely useful for investigations of carbon nanotubes. This method holds promise for the experimental investigation of special structural nanotube features, such as kinks, intertube junctions, or even tubes loaded with C_{60} molecules.

ACKNOWLEDGMENT

The authors wish to thank M. Beversluis and A. Bouhelier for stimulating discussions. Assistance on the CVD of SWNT's by Dr. T. Rueckes and Dr. B. Segal of Nantero (Woburn, MA) is gratefully acknowledged. This research was supported by NSF through grant BES-0086368.

REFERENCES

1. E. J. Sánchez, L. Novotny, and X. S. Xie, *Phys. Rev. Lett.* **82**, 4014 (1999).
2. K. Kneipp *et al.*, *Phys. Rev. Lett.* **78**, 1667 (1997).
3. S. Nie and S. R. Emory, *Science* **275**, 1102 (1997).
4. J. Wessel, *J. Opt. Soc. Am. B* **2**, 1538 (1985).
5. C. L. Jahncke, H. D. Hallen, and M. A. Paesler, *J. Raman Spectrosc.* **27**, 579 (1996).
6. R. M. Stöckle *et al.*, *Chem. Phys. Lett.* **318**, 131 (2000).
7. N. Hayazawa *et al.*, *Chem. Phys. Lett.* **335**, 369 (2001).
8. L. T. Nieman, G. M. Krampert, and R. E. Martinez, *Rev. Sci. Instrum.* **72**, 1691 (2001).
9. N. Hayazawa *et al.*, *J. Chem. Phys.* **117**, 1296 (2002).
10. A. Jorio *et al.*, *Phys. Rev. Lett.* **86**, 1118 (2001).
11. Z. Yu and L. Brus, *J. Phys. Chem. B* **105**, 1123 (2001).
12. G. S. Duesberg *et al.*, *Phys. Rev. Lett.* **85**, 5436 (2000).
13. J. Maultzsch, S. Reich, and C. Thomsen, *Phys. Rev. B* **65**, 233402 (2002).
14. K. Kneipp *et al.*, *Phys. Rev. Lett.* **84**, 3470 (2000).
15. K. Karrai and R. D. Grober, *Appl. Phys. Lett.* **66**, 1842 (1995).
16. M. J. Vasile, C. Biddick, and H. Huggins, *Appl. Phys. Lett.* **64**, 575 (1994).
17. L. Novotny, E. J. Sánchez, and X. S. Xie, *Ultramicroscopy* **71**, 21 (1998).
18. B. Sick, B. Hecht, and L. Novotny, *Phys. Rev. Lett.* **85**, 4482 (2000).
19. J. H. Hafner, C. L. Cheung, and C. M. Leiber, *J. Am. Chem. Soc.* **121**, 9750 (1999).
20. A. G. Souza Filho *et al.*, *Phys. Rev. B* **65**, 085417 (2002).
21. A. Jorio *et al.*, *Phys. Rev. Lett.* **85**, 2617 (2000).
22. C. Journet *et al.*, *Nature* **388**, 756 (1997).
23. A. M. Michaels, M. Nirmal, and L. E. Brus, *J. Am. Chem. Soc.* **121**, 9932 (1999).
24. E. J. Ayars, H. D. Hallen, and C. L. Jahncke, *Phys. Rev. Lett.* **85**, 4180 (2000).